Recent Advances in the Preparation and Performance of Porous Titanium-Based Anode Materials for Sodium-Ion Batteries

Athinarayanan Balasankar [1], Sathya Elango Arthiya [2], Subramaniyan Ramasundaram [3,*], Paramasivam Sumathi [4], Selvaraj Arokiyaraj [5], Taehwan Oh [3], Kanakaraj Aruchamy [3,*], Ganesan Sriram [3,*] and Mahaveer D. Kurkuri [6]

1   Department of Physics, Gobi Arts & Science College, Gobichettipalayam, Erode 638 453, Tamilnadu, India
2   Centre for Nano Sciences & Technology, Madanjeet School of Green Energy Technologies, Pondicherry University (A Central University), Puducherry 605 014, India
3   School of Chemical Engineering, Yeungnam University, Gyeongsan 38541, Republic of Korea
4   Department of Chemistry, Gobi Arts & Science College, Gobichettipalayam, Erode 638 453, Tamilnadu, India
5   Department of Food Science & Biotechnology, Sejong University, Seoul 05006, Republic of Korea
6   Centre for Research in Functional Materials (CRFM), Jain Global Campus, JAIN University, Bengaluru 562112, Karnataka, India
*   Correspondence: ramasundaram79@hotmail.com (S.R.); a.kanakaraj@yu.ac.kr (K.A.); sriramyu@yu.ac.kr (G.S.)

Abstract: Sodium-ion batteries (SIBs) are among the most cost-effective and environmentally benign electrical energy storage devices required to match the needs of commercialized stationary and automotive applications. Because of its excellent chemical characteristics, infinite abundance, and low cost, the SIB is an excellent technology for grid energy storage compared with others. When used as anodes, titanium compounds based on the Ti^{4+}/Ti^{3+} redox couple have a potential of typically 0.5–1.0 V, which is far from the potential of dangerous sodium plating (0.0–0.1 V). This ensures the operational safety of large-scale SIBs. Low lattice strain, usually associated with Ti-based materials, is also helpful for the longevity of the cycling of SIBs. Numerous Ti-based anode materials are being developed for use in SIBs. In particular, due to adequate electrode–electrolyte interaction and rapid charge transportation, hierarchical porous (HP) Ti-based anode materials were reported as having high specific capacity, current density, and cycling stability. HPTi-based anode materials for SIBs have the potential to be used in automobiles and portable, flexible, and wearable electronic devices. This review addresses recent developments in $HPTiO_2$-based SIBs and their preparation, properties, performance, and challenges.

Keywords: sodium-ion batteries; hierarchically porous TiO_2; titanium dioxide; anode materials; Ti nanomaterials

1. Introduction

The shortage of fossil fuels is increasing and an alternative is necessary to switch from nonrenewable to renewable energy sources, such as ocean energy, wind, solar, thermal, and geothermal [1–3]. Moreover, the climate has been changing due to pollution, resulting in an increase in pollution as well as global warming [4]. Carbon and harmful gases emitted from automobiles and industries are inducing global warming [5,6], which is considered a potential threat to the world, causing health issues, floods, and droughts. Batteries, a major energy storage device, have been considered as having the potential to control and reduce the damage being caused to the environment [7]. The most recent example is electric vehicles equipped with batteries [8]. Based on usage, batteries are categorized into two types: (1) primary batteries and (2) secondary batteries [9,10]. Primary batteries are nonrechargeable, but the secondary batteries are rechargeable and can be used for prolonged periods of time. This review deals with secondary batteries.

Based on the material source used, the secondary batteries are further divided into several types: lead-acid [11], aluminium-ion [12], dual carbon [13], vanadium redox flow [14], magnesium-ion [15], lithium-ion [16,17], sodium-ion [18,19], etc. Sodium (Na)-ion batteries are being developed as an economic replacement, as lithium batteries cost more [20]. The foremost advantage of sodium-ion batteries is that they are more abundant naturally and are less expensive than lithium. In the crust of the earth, sodium is present at 2.6%, while lithium is present at a much lower 0.06%. Compared with Li, which has an extraction cost of USD 5000 per ton, Na has a much lower cost of USD 150 per ton. Additionally, the cathode materials for Na-ion batteries contain abundant and environmentally safe materials instead of cobalt and nickel [21]. The most prominent anode material for batteries is graphite, which has a distinct layered structure, good cycling stability, a flat potential profile, high conductivity, and high coulombic efficiency [22]. However, its applicability in sodium-ion batteries is constrained by the small interlayer spacing and poor rate capability [23]. In addition, they are limited by the inability of reversible insertion/extraction of sodium ions [24]. Moreover, sodium-ion batteries have been intensively researched to replace expensive charge carriers with less expensive alternatives [25]. In order to improve the efficiency and energy storage in Na-ion batteries, titanium (Ti)-based materials and nanostructures have been synthesized. When used as anodes, titanium compounds based on the Ti^{4+}/Ti^{3+} redox couple have a potential of typically 0.5–1.0 V, which is far away from the potential of dangerous sodium plating (0.0–0.1 V). This ensures the operational safety of large-scale SIBs.

In the Earth's crust, Ti is widely distributed because it is one of the rock-forming elements. TiO_2 is nontoxic, stable, and inexpensive [26]. In nature, TiO_2 exists in four crystal structures, namely brookite, rutile, anatase, and bronze [27]. The sodiation/desodiation mechanism for different TiO_2 polymorphs is different and still unclear. It was recently studied only for anatase [28–30]. The conductivity of TiO_2 is low, which affects the performance of Na-ion batteries [31]. To overcome these disadvantages, multiple methods are being developed to prepare materials with varying morphology, control, size, and doping with heteroatoms [32–35].

2. TiO₂ as Anode Materials

For the first time, in 1991, Sony established commercialized Li-ion batteries (LiBs) in the energy storage market, whereas hard carbon and layered $LiCoO_2$ were utilized as anode and cathode materials, respectively [36]. Graphite was used as an anode material for LiBs instead of hard carbon. Due to increasing power demands, researchers focused on developing advanced batteries with higher storage capacity, power, and safety.

Graphite has safety issues in high-performance batteries [37,38]. To overcome the safety issues, graphite has been successfully replaced by lithium titanium oxide (LTO) [39] in the anode terminal. TiO_2 was proposed to replace LTO to increase the energy density of LIBs [40]. In this regard, the properties of TiO_2, such as electrochemical stability, low cost, and large-scale availability, are advantageous for battery applications [41]. Among the valve materials, TiO_2 possesses the highest stability [42,43]. Ti surfaces always have a thin, formed, natural oxide layer (TiO_2) due to their easy reaction with oxygen in the atmosphere [44]. Hence, the formation of TiO_2 can be achieved via simple, cost-effective, and eco-friendly procedures [45–47]. Upon calcination, TiO_2 with varying surface and crystalline features can be obtained. High-performance batteries require high storage density, which is associated with a short diffusion distance. To minimize the diffusion distance, Lewis et al. proposed a strategy of increasing the effective surface area of anode materials by using nanostructured TiO_2 [48]. The nanostructures rendered a remarkable Li storage value of 1.01–0.5 Li^+ [48]. Additionally, the effectiveness of several TiO_2 nanostructured morphologies as LiB anode materials was explored. Wu et al. achieved a maximum performance of 150 mAhg^{-1} and acycle performance of 100 mAhg^{-1} at the 70th cycle by using TiO_2 nanocrystals as anode materials [49]. Su et al. used TiO_2 anatase hollow nanospheres as anode materials in SIBs, and they obtained a maximum performance of 265 mAhg^{-1} [50]. TiO_2 nanorods were used as anode materials, and the maximum performance was about

220 mAhg^{-1}. Only nanosized particles were interacting with the electrolyte, resulting in another electrochemical reaction [51]. It may be the reason for the difficulties associated with reaching high power in SIBs. Therefore, the mixed micro/nano structure of TiO$_2$ has received attention. Table 1 demonstrates the electrochemical performance of hierarchically micro/nanoporous TiO$_2$ anode materials for SIBs.

Table 1. Electrochemical performance of hierarchically micro/nanoporous TiO$_2$ anode materials for SIBs.

Characteristics	Maximum Rate Performance (mAhg^{-1})	Cycle Performance (mAhg^{-1})	Strategy	Ref.
HP Li$_4$Ti$_5$O$_{12}$	165	121 at 30C (500 cycles)	Temperature-dependent rate capability of SIBs	[52]
Porous anatase TiO$_2$-HP structure	255.98	112.93 at 5C (100 cycles)	Low-cost yeast cells used as bio-templates	[53]
NaTi$_2$(PO$_4$)$_3$, nanoparticles	121	103 at 2C (300 cycles)	Cost-effective hydrothermal method without calcination	[54]
HP and high-tap-density TiO$_2$ spheres with controllable size	189	184 at 1C (200 cycles)	Hydrolysis method for producing different types of high-tap-density TiO$_2$	[55]
TiO$_2$ porous cake-like	250	173 (2500 cycles)	Annealing Ti-based metal-organic frameworks templates	[56]
TiO$_2$ free-standing HP nanocrystals	100	150 (500 cycles)	Mixing of multiwall carbon nanotubes and free-standing TiO$_2$ nano crystals by ubes (designated as TiO$_2$ MWCNTs) for Na storage by free-drying, annealing, and modified vacuum filtering	[57]
TiO$_2$ HP nanopills	196.4	115.9 (3000 cycles)	MIL-125(Ti) titanium metal–organic framework as a precursor	[58]
Flower-like ultrathin TiO$_2$ nanosheets composed of anatase and bronze	120	104 at 100C (6000 cycles)	Simple solvothermal reaction and high temperature annealing	[59]
Self-assembled hierarchical spheroid-like KTi$_2$(PO$_4$)$_3$@C nanocomposites	283.2	136.1 (5000 cycles)	Electrospray method	[60]
TiO$_2$ nanoparticles linked in consistent pattern to compose HP hybrid nanosheet	146	129 at 10C (20,000 cycles)	Adding nitrogen-doped graphene layer networks	[61]
HP anatase TiO$_2$ microparticles	275	40 at 10C (450 cycles)	Incorporation of organic surface modifiers with supercritical methanol (scMeOH)	[62]
Hierarchical architecture of porous anatase TiO$_2$ microspheres	207.3	140.6 (10,000 cycles)	Solvothermal reaction, combining ether-based electrolyte with porous structure	[63]
TiO$_2$/MoS$_2$ to form a nanoflower structure	616	460 (350 cycles)	Construction of hybrid architecture composed of MoS$_2$ and TiO$_2$ nanosheets	[64]

Figure 1 shows the structure of nanoporous and hierarchically micro/nanoporous TiO$_2$ anodes and associated preparation methods. The material's active surface area is important to obtain batteries with high charge storage parameters. Thus, porous materials, especially nanoporous ones, were developed. Table 2 compares the performance of nanoporous TiO$_2$ made using different methods for use in Na-ion batteries. In this material, nanopores are connected by a very thin wall of TiO$_2$. Thin walls of TiO$_2$ are highly prone to react with electrolytes and gradually detach from the anode terminal. Disintegration of the anode structure decreases the overall performance of SIBs. Additionally, hierarchically structured micro/nanoporous (HMNP) surfaces endow better binding energy and a high surface-to-volume ratio and prevent the undesirable electrochemical reaction between the electrode and TiO$_2$. Thereby, the performance of SIBs can be maintained over a prolonged usage cycle. HMNP TiO$_2$ can be fabricated by several methods, including the sol-gel route, coprecipitation, metal–organic framework, vacuum filtration process, and electrospray.
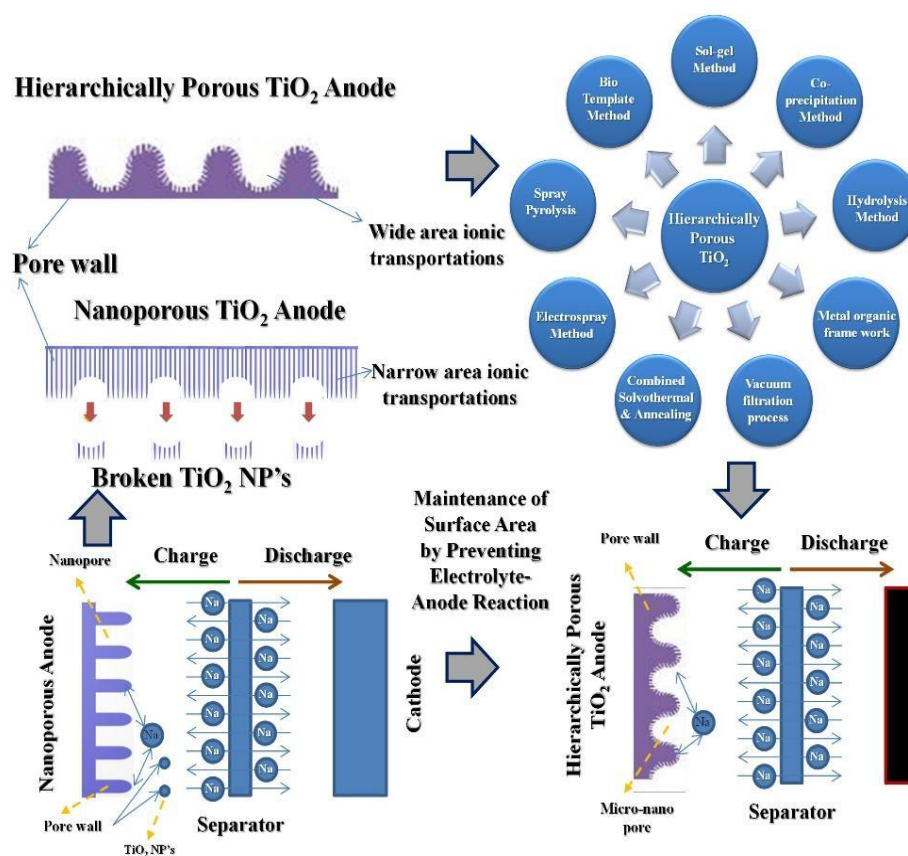
Figure 1. Schematic of HPTiO$_2$ anode materials, existing preparation methods, and advantages.

**Table 2.** The electrochemical performance of nanoporous TiO$_2$ as anode materials for SIBs.

Characteristics	Maximum Rate Performance (mAhg^{-1}/Ag^{-1})	Cycle Performance (mAh g^{-1})	Strategy	Reference
Porous TiO$_2$ nanospheres	123.1/4.0	208 (over 500 cycles)	Graphene-supported TiO$_2$ nanospheres by using hydrothermal method	[65]
Nanoporous anatase TiO$_2$	179/6.7	145 at 1C (over 3000 cycles)	Combination of uniforme nanopores and tiny nanocrystals	[66]
TiO$_2$ nanotubes	257/0.05	103 (over 700 cycles)	Sn doping	[67]
Mesoporous TiO$_2$(B)	For Zn-doping 173/0.05 For nickel-doping 104/1.8	For Zn-doping 151 (over 100 cycles) For nickel-doping 97 (over 50 cycles)	Zn doping, nickel doping	[68]
Mesoporous TiO$_2$	150/2	135–150 (over 100 cycles)	Anode material prepared by using anatase TiO$_2$ nanocrystals	[69]
Nanoporous NaTi$_2$(PO$_4$)$_3$//Na$_3$V$_2$(PO$_4$)$_3$	85/2.4	64 (over 1000 cycles)	Scalable sol-gel method	[70]

3. Methods of Preparing Hierarchical Micro/Nanoporous Structured Ti-Based Materials

3.1. Sol-Gel Route

Low cost, improved power density, and efficiency are major requirements for an anode. For example, Li$_4$Ti$_5$O$_{12}$ [52] monolith was synthesized by treating TiO$_2$ gels (tunable macro-porous) in aqueous LiOH, and subsequent calcinations at 700–800 °C. The resultant flower-like nanostructures exhibited a performance of 146 mAhg^{-1} at 10C and 105 mAhg^{-1} at 30C, without carbon coating. When applied as an anode in SIBs, this material improved

the operating temperature. Figure 2 displays the morphology of the obtained nanostructures after each step. As previously stated, hydrous lithium titanate (LHLT) particles are produced on the surface of macropores by treating porous TiO_2 gels in aqueous LiOH under moderate conditions. Though subjected to a high-temperature calcination process, crack-free, monolithic, flower-like structures with interconnected macroporous structure are preserved. The flower-like structures have a thickness of ~30 nm and have granular crystallites of 30–80 nm in diameter. The rod-like structures were obtained at 800 °C due to sintering-induced densification. An increase in the number of active sites increased the rate-capability performance.
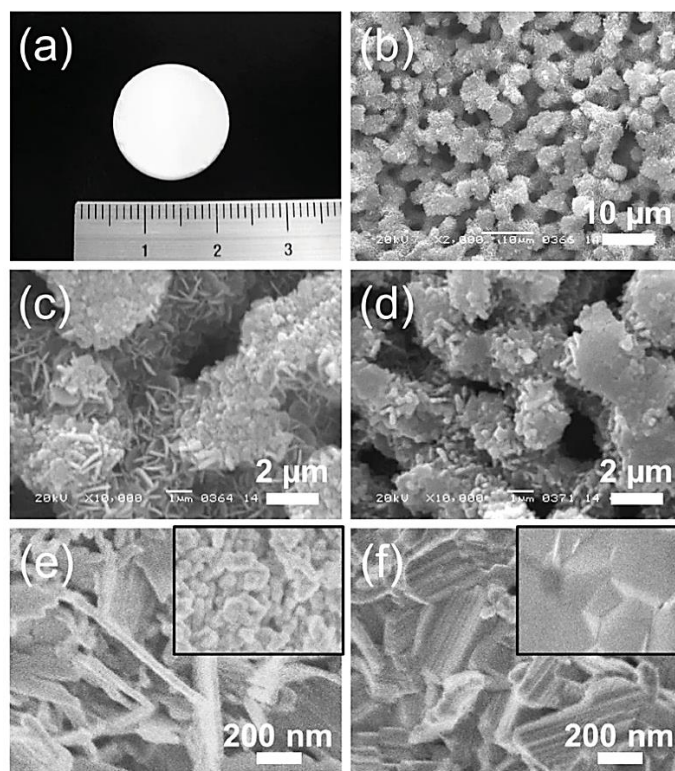

Figure 2. (**a**) Appearance of the monolithic $Li_4Ti_5O_{12}$ calcined at 700 °C. (**b**–**f**) SEM image samples calcined at 700 and 800 °C: (**b**,**c**,**e**) samples calcined at 700 °C; and (**d**,**f**) samples calcined at 800 °C. Insets in (**e**) and (**f**) are respective cross-sectional images [52].

3.2. Coprecipitation

The phosphates in NASICON (Na superionic conductor) have the general formula $AxMM'(PO4)_3$; for example, $KTi_2(PO_4)_3@C$ has a 3D-framework structure. This material structure provides fast ion interactions and fast extractions. Because of its low cost and high safety compared with aqueous Na-ion-based batteries, superionic conductor structures of sodium titanium phosphate ($NaTi_2(PO_4)_3$) were synthesized [54] and subjected to a carbon coating process. $NaTi_2(PO_4)_3$ was formed as a NASICON structure with good crystallinity and high phase purity. For electrochemical evaluations, under ambient conditions, a 1 M Na_2SO_4 aqueous electrolyte, NTP5h/C anode, and $Na_{0.44}MnO_2$ cathode were assembled.

The initial charge and discharge capacities based on NTP mass were 131 and 121 mAh g^{-1}, respectively, as shown in Figure 3a,b, equating to a coulombic efficiency of 92%. The remarkable reversibility was ascribed to its open 3D framework inside the NTP structures, better aqueous electrolyte kinetics, and rapid Na ion transport. Discharge capabilities at different rates were measured. When the rate was increased to 2C, the discharge capacity was determined to be around 103 mAh g^{-1}, which is 85% of the value reported. In terms of cycling performance, Figure 3c shows that after 300 cycles at 1C at voltages ranging from 0.7 to 1.3 V, the cell had around 75% cyclic stability and >99.5% coulombic efficiency. Electrochemical

impedance spectra between 1 MHz and 10 mHz, measured after 10, 30, and 50 cycles of 100% discharge, each had an amplitude of 10 mV (Figure 3d). In comparison with the fitted RCT values (i.e., $[R_s + R_{CT}]$—$[R_s]$), it can be noticed that the RCT value of the NTP 5h/C slightly decreased upon cycling, i.e., 2.3 Ω at the 10th cycle and 2.1 Ω at the 50th cycle. This promoted electronic conductivities. In addition, they possessed rate capability, high reversible capacity, and cycling performance. Apart from these advantages of NASICON, however, there are some disadvantages, such as its low electronic conductivity ($>10^{-12}$ Scm^{-1}) and slow kinetic property. Therefore, it failed to reach its theoretical capacity [60].
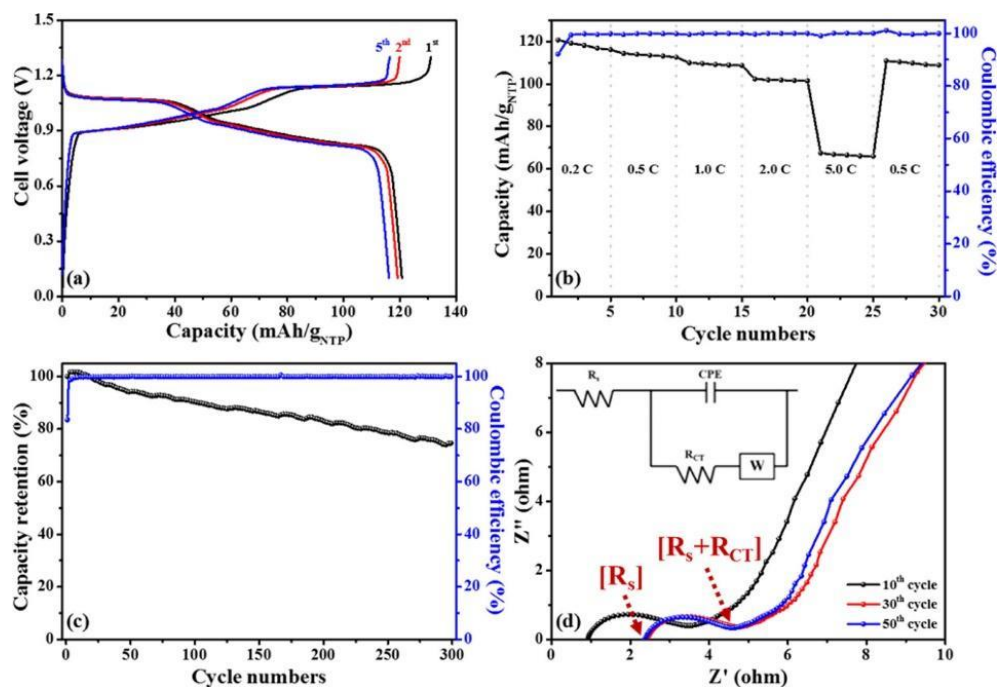
**Figure 3.** (**a**) Capacity, (**b**) rate capability, (**c**) cycle performance, and (**d**) electrochemical impedance spectra of the NTP-5h/C. For (**a**) and (**c**), the C rates employed were 0.2 C and 1 C, respectively. The analogous circuit model utilized for the parameter-fitting is shown in (**d**) [54].

3.3. Hydrolysis Route

Hydrolysis of a precursor mixture containing graphite oxide, hydrogen peroxide, NH$_3$ H$_2$O [55], different high-tap-density TiO$_2$ spheres, and nanograins with hierarchical porous structure were synthesized, the morphology of which is shown in Figure 4. Hydrolysis at 80 °C and annealing in an Ar atmosphere at 450 °C resulted in crystalline TiO$_2$ spheres having a typical size of 500 nm. The size was further decreased to 100–150 nm TiO$_2$. The addition of ethanol and changes in the concentration of Ti(OH)$_4$ yielded different sizes of TiO$_2$ spheres. As the volume ratio of the precursor solution to the ethanol reduced from 2:1, 1:1, 1:2, to 1:4, the average diameter of the TiO$_2$ spheres steadily shrunk from approximately 1.5 μm to 100 nm. Many nanospheres, each with a diameter of 90 nm from the TiO$_2$ sample, contained a few microspheres; this is schematically explained in Figure 5. The as-synthesized material had improved storage and transportation properties. At 1 C, the Na-ion storage specific capacity was found to be 184 mAh g^{-1} with a capacity retention of 90.5% after 200 cycles.
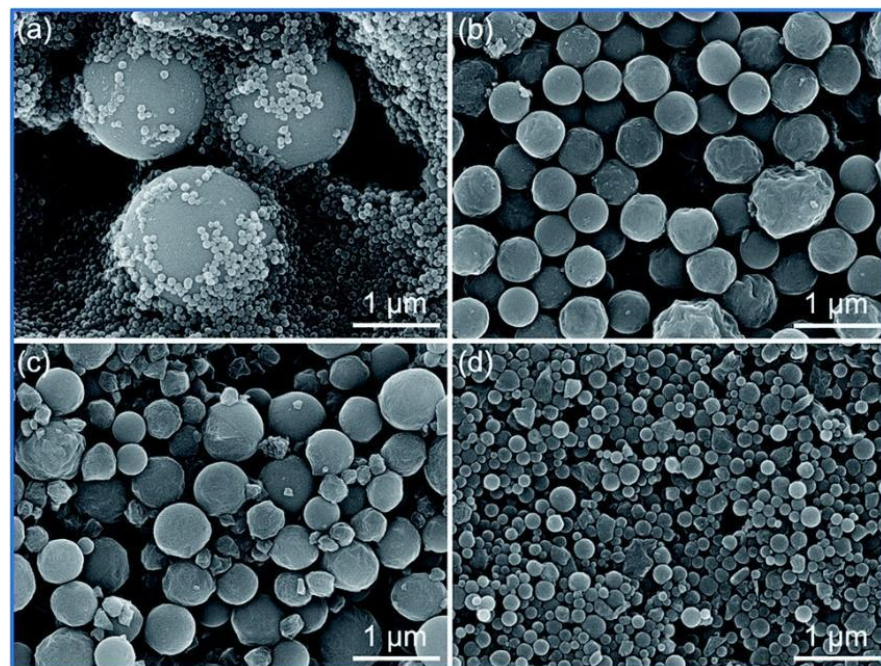
Figure 4. Four TiO$_2$ spheres were imaged using SEM: (**a**) TiO$_2$ (2:1), (**b**) TiO$_2$ (1:1), (**c**) TiO$_2$ (1:2), and (**d**) TiO$_2$ (1:4). Parentheses indicate the ratios of the precursor to the absolute alcohol in each TiO$_2$ sphere [55].
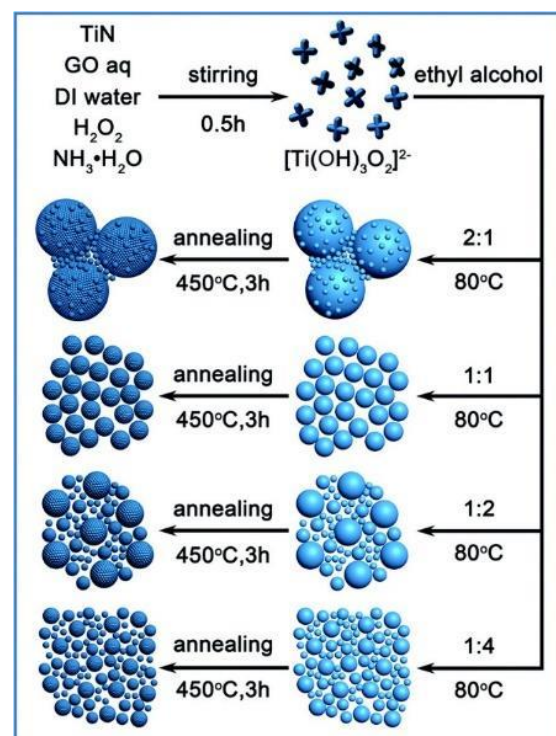
Figure 5. Diagrammatic representation of the synthesis of four TiO$_2$ spheres with different sizes by adjusting the volume ratios of the precursor solution consisting of GO, H$_2$O$_2$, and NH$_3$ H$_2$O to absolute ethanol [55].

3.4. Metal-Organic Framework (MOF)

Simple synthesis methods are still required to improve the properties and to make it cost-effective. TiO$_2$ with a porous cake structure [56] was synthesized by simple annealing of Ti-based metal-organic templates. All the corresponding tests were conducted such

as X-ray diffraction, nitrogen adsorption-desorption, galvanic charge, or discharge tests. The maximum charge capacity was to be found to be 250 mAhg^{-1} after 50 cycles, and 50 mAhg^{-1} of charge density provided stable reversible capacity. An excellent electrochemical performance was observed (Figure 6).

TiO$_2$ nanopills were synthesized using a titanium metal-organic framework [58]. These nanopills had a high specific surface area of 102 m^2/g. When the material was employed as an anode in SIBs, it provided good results with a discharge capacity of 196.4 mAh g^{-1} at a current density of 0.1 Ag^{-1}. The capacitive retention was 90% after 3000 cycles. Figure 7 shows the Na$^+$-ion storage and diffusion in hierarchically porous TiO$_2$ nanopills.
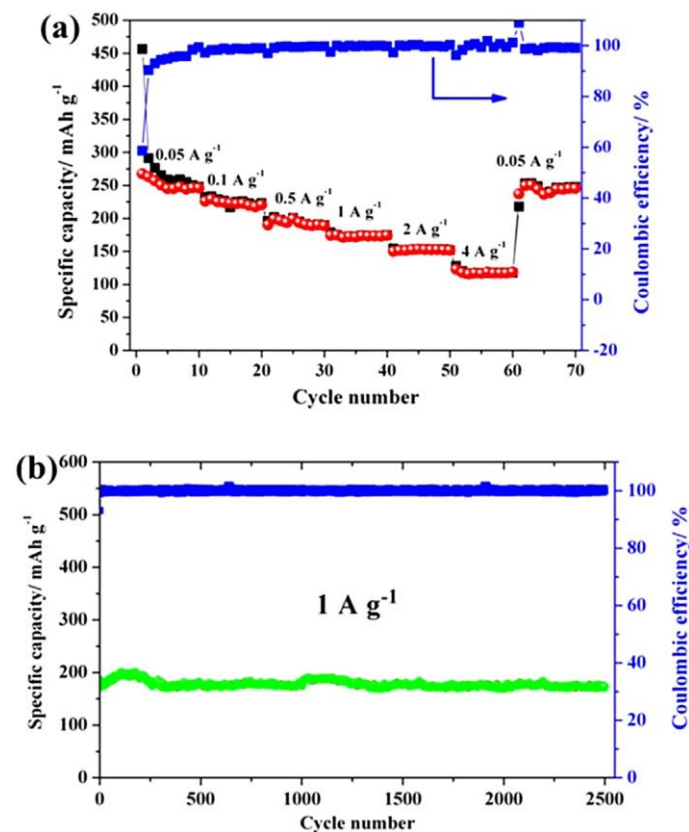

Figure 6. (**a**) Rate performance at various current densities, and (**b**) long-life cycling performance of powder of porous TiO$_2$ at 1Ag^{-1} [56].

3.5. Vacuum Filtration Process

Different types of hierarchical structures were designed to determine their performance. Liu et al. prepared freestanding HP assemblies from TiO$_2$ nanocrystals and multiwalled nanotubes (MWCNTs) [57]. Figure 8 shows a schematic representation of commercially viable and low-cost methods for obtaining free-standing TiO$_2$-MWCNT assemblies. TiO$_2$ nanocrystals (60 mg) were dispersed in 0.5% bovine serum albumin, then the BSA-coated TiO$_2$ nanocrystals were mixed with 1 mg/mL of oxidized MWC-NTS. This composite was redispersed in 1 mg/mL NH$_4$HCO$_3$ and stirred to yield a fluffy TiO$_2$/MWCNTs intermediate. Upon filtration and two-step heat treatment (600 °C for 6 h and 350 °C for 2 h) annealing at free-standing TiO$_2$-MWCNTs assembly was obtained. The packing density of this assembly was 0.63 g cm^{-3}. The TiO$_2$-MWCNTs assembly was found to be mechanically stable and possess high electrical conductivity. Apart from flower-like structures, nanotubes and nanoparticles were also explored.
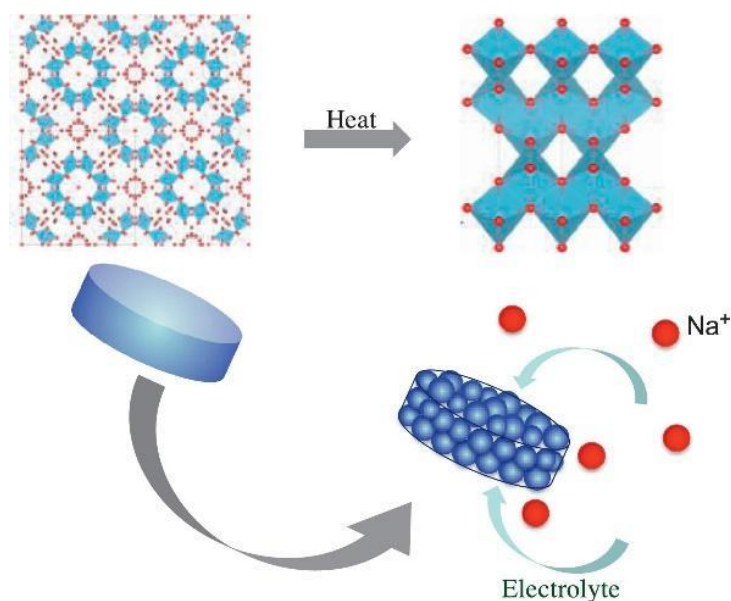
Figure 7. Na⁺-ion storage and diffusion in hierarchically porous TiO$_2$ nanopills.
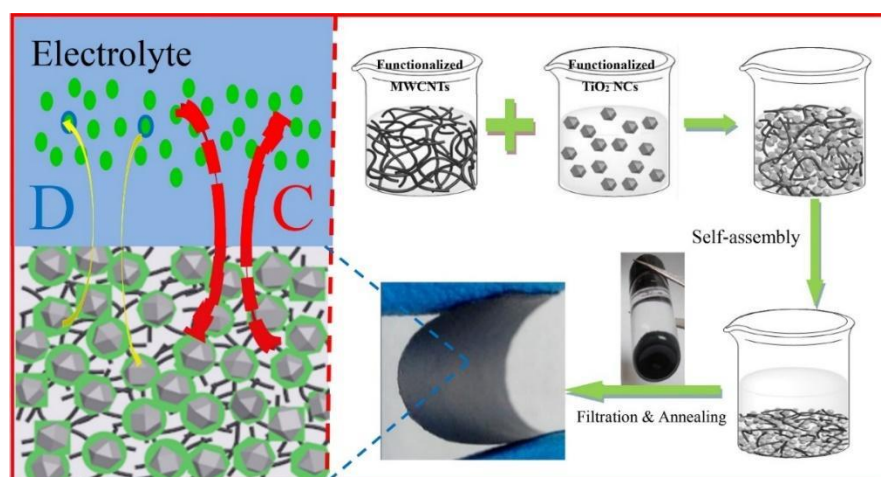
Figure 8. An example of a schematic showing the steps involved in creating a free-standing TiO$_2$ MWCNT electrode with routes for salt storage. "D" and "C" represent sodium storage behavior that is diffusion-controlled and capacitive (due to the interfacial Na storage process) [57].

3.6. Combined Techniques of Solvothermal and Annealing Process

Ultrathin nanosheets with a flower structure assembly consisting of anatase/bronze type TiO$_2$ in carbon were reported [59]. The synthesis process consisted of a solvothermal process and subsequent annealing at high temperatures. Excellent electrochemical properties were observed. Apart from structure-driven performance improvement, the carbon matrix and the interface between anatase and carbon structure also enhanced the overall efficiency. Figure 9 shows the hypothesis model sodium storage at the TiO$_2$(A)/TiO$_2$(B) interface.
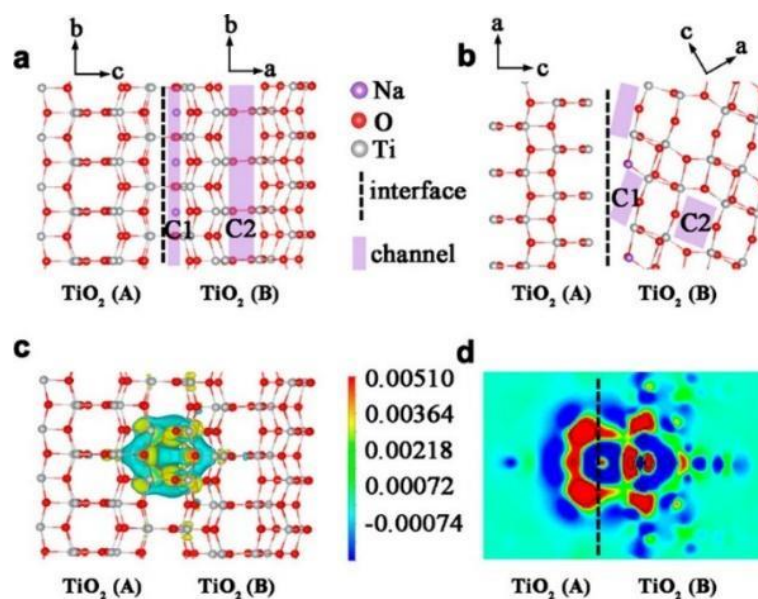
Figure 9. (**a**) A hypothesis about the storage of sodium at the $TiO_2(A)/TiO_2(B)$ interface. Relaxed interfacial structure doped with Na in the [100] and [001] directions of $TiO_2(A)$ and $TiO_2(B)$, or in the [010] and [100] directions of $TiO_2(A)$ and $TiO_2(B)$ (**b**). (**c**,**d**) The change in charge density at the interface caused by Na doping. The red zone shows an accumulation of density, the blue region shows a depletion of electron density. (A) and (B) correspond to the anatase and bronze crystal structures of TiO_2, respectively; a, b, and c stand for lattice parameters [59].

3.7. Coating Techniques

In order to attain efficient energy storage in SIBs, various materials were coated on TiO_2-based hierarchical nano and microporous anode materials. Li et al. prepared nitrogen-doped graphene nanosheets and TiO_2 composites with an interconnected structure having a layered network [61]. This composite functioned as both a self-sacrificial template and as a hybrid carbon source and provided the longest cyclabilities. Wei et al. [60], fabricated potassium titanyl phosphate and a carbon-based porous composite (KTP@C). The schematics of the synthesis and morphology of this composite are shown in Figure 10. Because charged droplets were present throughout the electrospray procedure, microspheres could be observed and were clearly dispersed in the TEM and SEM pictures displayed. The KTP@C composite was heated for four hours at 800 °C. In Figure 10d,e, nanoscale particles (between 50 and 300 nm) are depicted, and the average spherical size ranged from 1 to 4 m (see the inset in Figure 10d). The spheres were self-assembled aggregates of KTP nanoparticles, according to the TEM images in Figure 10f,g.

HP anatase TiO_2 microparticles were synthesized by using supercritical methanol with organic surface-modifying substances such oleic acid. Porous anatase TiO_2 was also prepared by typical solvothermal methods as it improved electronic or ionic transport, cyclic stability, and other properties [62,63]. As mentioned earlier, in terms of the Na^+-ion storage mechanism in the carbon-coated TiO_2 particles (CPC-TiO_2, which was prepared by using citric acid (CA) and polyethylene glycol methyl ether (PEGME)) electrode, electronic impedance spectra were obtained during the first processes of sodiation and desodiation (Figure 11a,b). When sodiation and desodiation first began, the electrolyte impedance (Re) levels were low. When the insertion of the Na^+ ion occurred at 0.005 V, the RSEI values steadily climbed to 123.97 Ω. Then, they gradually dropped to 39.27 Ω upon electrode desodiatation. The potential profile depicted in Figure 11a was produced by the solid electrolyte interphase layer formation at close to 0.5 V during sodiation.

Ex situ XRD analysis was used to better explore CPC-sodium TiO_2's storage behavior (Figure 11c). Prior to cycling shifting to 25.130, the (101) plane's apex was visible at 25.250. Prior to cycling, the peak of the (200) plane was at 48.210, it changed to 48.260 at 0.005 V

during sodiation, and it returned to the initial values at 2.5 V after the electrode was fully desodiated. The Na^+-ion uptake by the CPC-TiO_2 and the Na^+-ion insertion into the TiO_2 phase are both influenced by the interfacial storage.
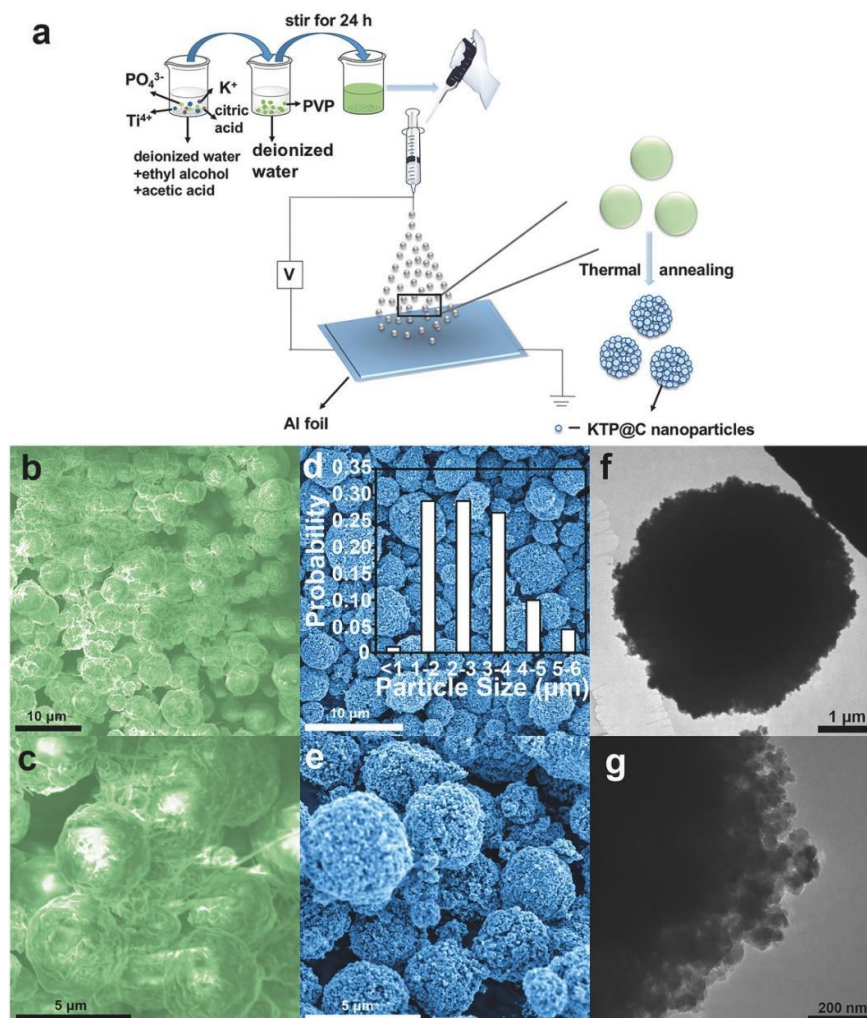

Figure 10. (**a**) Synthesis diagram for KTP@C nanocomposites; (**b–g**) morphology of SEM of KTP@C; (**b,c**) precursor as sprayed; different resolutions of KTP@C nanocomposites are shown in (**d,e**). The KTP@C's grain size distribution is shown in the inset in (**d**), and the KTP@C's TEM image is shown in (**f,g**) [60].

3.8. Template-Assisted Spray Pyrolysis

The cow electronic conductivity and drastic volume of the cycles of batteries lead to decaying capacity and poor structural stability. So, the intercalation TiO_2 materials or hybrid structure materials for anode have gained popularity due to their affordable price and strong stability. In the case of hybrid nanoflowers and nanosheets, the structure of TiO_2/MoS_2 has improved the mobility of Na^+ ions during charge and discharge cycles. These materials can be synthesized by the template-supported spray pyrolysis method or by the hydrothermal and calcination method [64,71].

The morphology of TiO_2/MoS_2 is shown in Figure 12a–c. The samples of TiO_2:MoS_2 with lattice spacings of 1:0.5, 1:1, and 1:1.5 had respective lattice spacings of 0.35, 0.37, and 0.35 nm. Figure 12d indicates the XRD patterns of these three samples. Two identified peaks at 464.46 eV and 458.71 eV, corresponding to the Ti $2p_{3/2}$ and Ti $2p_{1/2}$ orbitals, respectively, and two peaks of binding energy with an interval of 5.75 eV are visible in the 1:1 sample of the Ti 2p XPS spectra seen in Figure 12e. The aforementioned findings demonstrated that the electron density around Ti^{4+} was reduced, leading to a decrease in the binding energy.
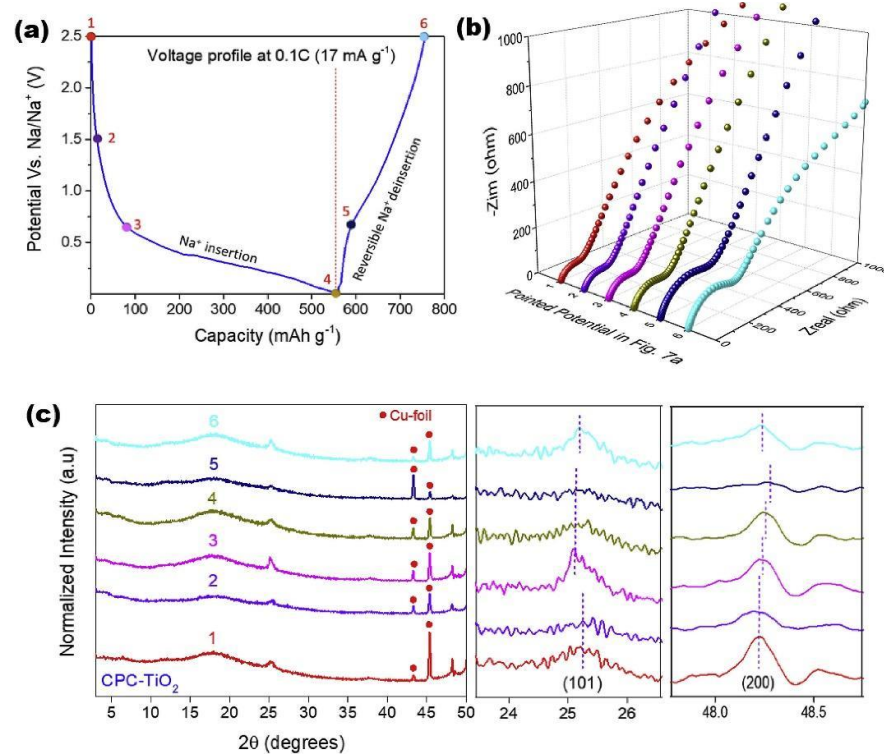
Figure 11. (**a**) Galvanostatic voltage pattern, (**b**) Nyquist plot, and (**c**) ex situ XRD plots during the initial sodiation and desodiation processes of CPC-TiO₂ [62].
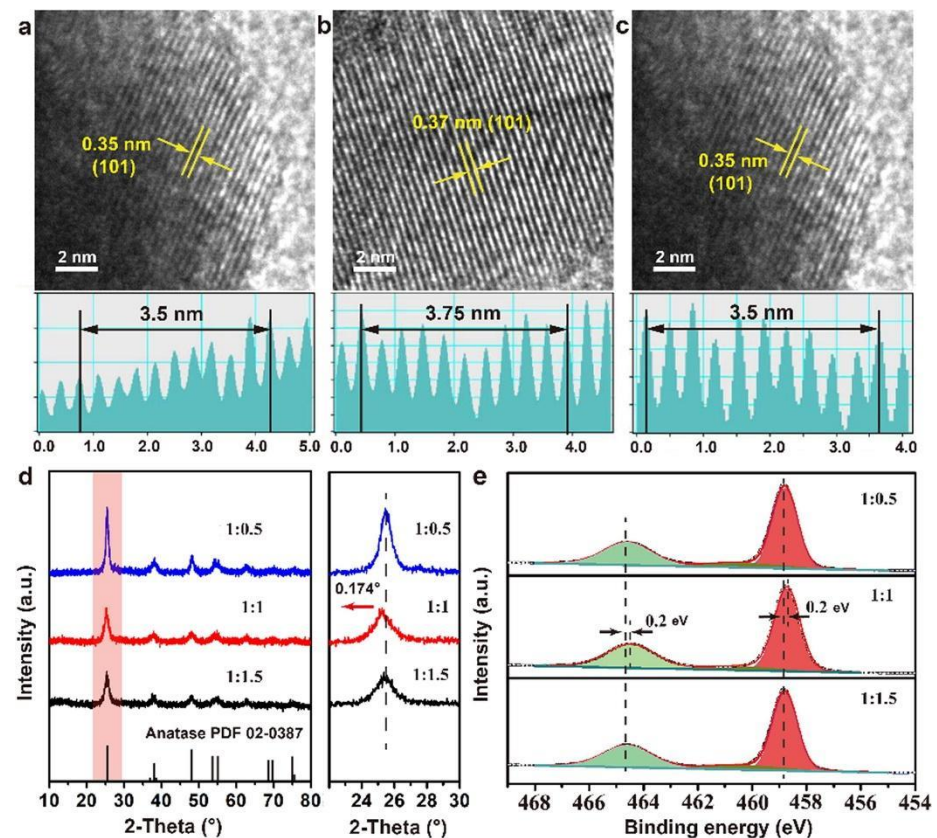
Figure 12. (**a**–**c**) High-resolution TEM images of the 1:0.5, 1:1, and 1:1.5 (TiO₂:MoS₂) samples, respectively; (**d**) XRD patterns and (**e**) Ti 2p XPS spectra of the above three samples [71].

3.9. Biotemplate Route

TiO_2-based anode materials were also prepared using biotemplates. For example, a yeast biotemplate [53] was used to prepare a porous TiO_2 anode material. Figure 13 shows the significant FESEM images of the biotemplate yeast cells. Spheres with a diameter of 2.0–3.0 μm were formed. The surface of yeast cells was coated with spherical TiO_2 particles; the solid, porous TiO_2 was typically 1.5 to 2.5 microns in diameter and had pore walls that were 0.2 to 0.7 microns thick. According to Figure 13d, the very small primary nanoparticles filled the outer surface of the micropore. The produced porous TiO_2 material had a discharge capacity of 255.98 mAh g^{-1}, and after 100 cycles, capacity retention was around 80%. Ion diffusion was excellent due to the electrolyte's access to the electrode.
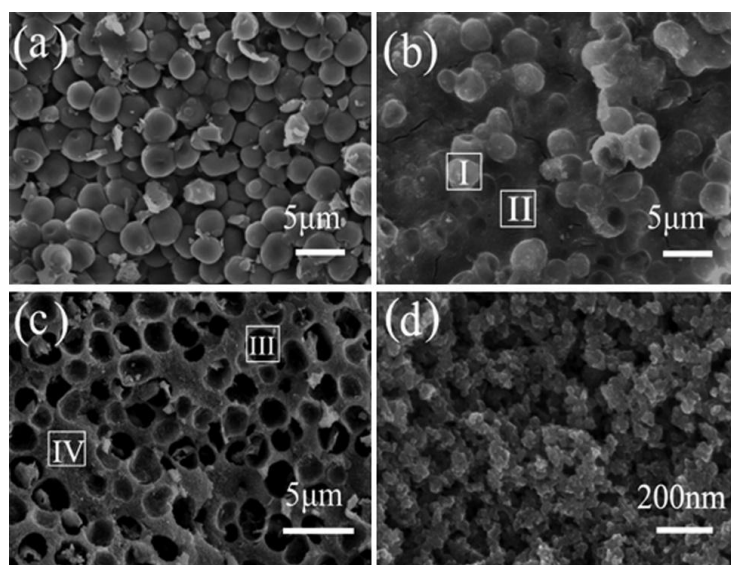
Figure 13. FESEM micrographs of yeast cells (**a**), yeast@TiO_2 precursor (**b**), and its calcined sample TiO_2 (**c**,**d**) in air at 450 °C for 3 h. Points I and II in (**b**) and points III and IV in (**c**) were the points in which energy dispersive spectroscopy was studied for the calcined products [53].

4. Conclusions

The selection of electrode material was found to be one of the main factors important for obtaining high-performance SIBs. Hierarchical TiO_2 nanostructures-based anode materials were found to be useful for developing SIBs with high grid storage. HP TiO_2 anode materials were utilized for achieving long cycle ability without a sudden drop in rate performance in the SIBs. Generally, TiO_2-based anodes possess merits such as relatively high performance, cost-effectiveness, and higher stability than other materials used so far. In order to decrease the diffusion length by HP TiO_2 anodes in SIBs for various synthesis routes were used, such as sol-gel route, coprecipitation, hydrolysis route, vacuum filtration process, combined method of solvothermal and annealing process and coating techniques. These multiple developments of porous titania-based anode materials were focused on SIBs, and its anode material will improve performance and can be used for wide applications, completely replacing LIBs in the future. However, a few disadvantages are still present with the available fabrication route. They are expensive, time-consuming, use hazardous chemicals, and complicate the process to develop prototypes for mass production; these required parameters need to be studied by researchers. In general, all of those will be addressed and resolved by laser sintering 3D-printing technology in the future. Moreover, by preventing dangerous sodium plating, TiO_2-based anodes endow operational safety to SIBs. TiO_2 nanostructures were rendering SIBs with high current density, cyclic stability, and specific capacity along with less durability. In the case of SIBs with HP TiO_2 anodes, they have the potential to be used in wearable electronic devices and automobiles for achieving high mileage and long life in the near future.

References

1. Pimentel, D.; Marklein, A.; Toth, M.A.; Karpoff, M.; Paul, G.S.; McCormack, R.; Kyriazis, J.; Krueger, T. Biofuel impacts on world food supply: Use of fossil fuel, land and water resources. *Energies* **2008**, *1*, 41–78. [CrossRef]
2. Raugei, M.; Hutchinson, A.; Morrey, D. Can electric vehicles significantly reduce our dependence on non-renewable energy? Scenarios of compact vehicles in the UK as a case in point. *J. Clean. Prod.* **2018**, *201*, 1043–1051. [CrossRef]
3. Rahman, A.; Farrok, O.; Haque, M. Environmental impact of renewable energy source based electrical power plants: Solar, wind, hydroelectric, biomass, geothermal, tidal, ocean, and osmotic. *Renew. Sustain. Energy Rev.* **2022**, *161*, 112279. [CrossRef]
4. Ramanathan, V.; Feng, Y. Air pollution, greenhouse gases and climate change: Global and regional perspectives. *Atmos. Environ.* **2009**, *43*, 37–50. [CrossRef]
5. Hassoon, H.A. Measurement of carbon emissions from vehicles exhaust pipe using portable gas detector. *Iraqi J. Agric. Sci.* **2019**, *50*. [CrossRef]
6. Rehan, R.; Nehdi, M. Carbon dioxide emissions and climate change: Policy implications for the cement industry. *Environ. Sci. Policy* **2005**, *8*, 105–114. [CrossRef]
7. Palomares, V.; Serras, P.; Villaluenga, I.; Hueso, K.B.; Carretero-González, J.; Rojo, T. Na-ion batteries, recent advances and present challenges to become low cost energy storage systems. *Energy Environ. Sci.* **2012**, *5*, 5884–5901. [CrossRef]
8. Chen, M.; Ma, X.; Chen, B.; Arsenault, R.; Karlson, P.; Simon, N.; Wang, Y. Recycling end-of-life electric vehicle lithium-ion batteries. *Joule* **2019**, *3*, 2622–2646. [CrossRef]
9. Vincent, C.A. Lithium batteries: A 50-year perspective, 1959–2009. *Solid State Ion.* **2000**, *134*, 159–167. [CrossRef]
10. Murata, K.; Izuchi, S.; Yoshihisa, Y. An overview of the research and development of solid polymer electrolyte batteries. *Electrochim. Acta* **2000**, *45*, 1501–1508. [CrossRef]
11. Yang, J.; Hu, C.; Wang, H.; Yang, K.; Liu, J.B.; Yan, H. Review on the research of failure modes and mechanism for lead–acid batteries. *Int. J. Energy Res.* **2017**, *41*, 336–352. [CrossRef]
12. Das, S.K.; Mahapatra, S.; Lahan, H. Aluminium-ion batteries: Developments and challenges. *J. Mater. Chem. A* **2017**, *5*, 6347–6367. [CrossRef]
13. Ji, B.; Zhang, F.; Wu, N.; Tang, Y. A dual-carbon battery based on potassium-ion electrolyte. *Adv. Energy Mater.* **2017**, *7*, 1700920. [CrossRef]
14. Lourenssen, K.; Williams, J.; Ahmadpour, F.; Clemmer, R.; Tasnim, S. Vanadium redox flow batteries: A comprehensive review. *J. Energy Storage* **2019**, *25*, 100844. [CrossRef]
15. Huie, M.M.; Bock, D.C.; Takeuchi, E.S.; Marschilok, A.C.; Takeuchi, K.J. Cathode materials for magnesium and magnesium-ion based batteries. *Coord. Chem. Rev.* **2015**, *287*, 15–27. [CrossRef]
16. Wang, Y.; Yi, J.; Xia, Y. Recent progress in aqueous lithiumion batteries. *Adv. Energy Mater.* **2012**, *2*, 830–840. [CrossRef]
17. Opra, D.; Gnedenkov, S.; Sinebryukhov, S.; Podgorbunsky, A.; Sokolov, A.; Ustinov, A.Y.; Kuryavyi, V.; Mayorov, V.Y.; Zheleznov, V. Doping of titania with manganese for improving cycling and rate performances in lithium-ion batteries. *Chem. Phys.* **2020**, *538*, 110864. [CrossRef]
18. Yabuuchi, N.; Kubota, K.; Dahbi, M.; Komaba, S. Research development on sodium-ion batteries. *Chem. Rev.* **2014**, *114*, 11636–11682. [CrossRef]
19. Opra, D.; Gnedenkov, S.; Sokolov, A.; Podgorbunsky, A.; Ustinov, A.Y.; Mayorov, V.Y.; Kuryavyi, V.; Sinebryukhov, S. Vanadium-doped TiO2-B/anatase mesoporous nanotubes with improved rate and cycle performance for rechargeable lithium and sodium batteries. *J. Mater. Sci. Technol.* **2020**, *54*, 181–189. [CrossRef]
20. Chayambuka, K.; Mulder, G.; Danilov, D.L.; Notten, P.H. From li-ion batteries toward Na-ion chemistries: Challenges and opportunities. *Adv. Energy Mater.* **2020**, *10*, 2001310. [CrossRef]
21. Abraham, K. How comparable are sodium-ion batteries to lithium-ion counterparts? *ACS Energy Lett.* **2020**, *5*, 3544–3547. [CrossRef]
22. Hu, Y.-X.; Zhang, D.-T.; Tang, F.-L.; Tian, C.-Y.; Li, J.; Jin, X.; Chang, C.-G.; Liu, M.-C. Expanded interlayer spacing of graphene oxide achieved by electrostatic cation intercalation towards superior sodium ion storage. *Ionics* **2022**, *28*, 3833–3842. [CrossRef]
23. Guo, Y.; Zhang, L.; XiLi, D.; Kang, J. Advances of carbon materials as loaders for transition metal oxygen/sulfide anode materials. *Chin. J. Rare Met.* **2021**, *45*, 1241.
24. Meng, J.; Jia, G.; Yang, H.; Wang, M. Recent advances for SEI of hard carbon anode in sodium-ion batteries: A mini review. *Front. Chem.* **2022**, *10*, 986541. [CrossRef]

25.	Kim, H.; Kim, D.I.; Yoon, W.-S. Challenges and Design Strategies for Conversion-Based Anode Materials for Lithium-and Sodium-Ion Batteries. *J. Electrochem. Sci. Technol.* **2022**, *13*, 32–53. [CrossRef]

26.	Guo, S.; Yi, J.; Sun, Y.; Zhou, H. Recent advances in titanium-based electrode materials for stationary sodium-ion batteries. *Energy Environ. Sci.* **2016**, *9*, 2978–3006. [CrossRef]

27.	Wei, T.-T.; Wang, F.-F.; Li, X.-Z.; Zhang, J.-H.; Zhu, Y.-R.; Yi, T.-F. Towards high-performance battery systems by regulating morphology of TiO_2 materials. *Sustain. Mater. Technol.* **2021**, *30*, e00355. [CrossRef]

28.	Wu, L.; Bresser, D.; Buchholz, D.; Giffin, G.A.; Castro, C.R.; Ochel, A.; Passerini, S. Unfolding the mechanism of sodium insertion in anatase TiO_2 nanoparticles. *Adv. Energy Mater.* **2015**, *5*, 1401142. [CrossRef]

29.	Fehse, M.; Henry, A.; Zitolo, A.; Boury, B.; Louvain, N.; Stievano, L. Revisiting the Sodiation Mechanism of TiO_2 via Operando X-ray Absorption Spectroscopy. *Appl. Sci.* **2020**, *10*, 5547. [CrossRef]

30.	Lin, D.; Li, K.; Wang, Q.; Lyu, L.; Li, B.; Zhou, L. Rate-independent and ultra-stable low-temperature sodium storage in pseudocapacitive TiO_2 nanowires. *J. Mater. Chem. A* **2019**, *7*, 19297–19304. [CrossRef]

31.	He, H.; Gan, Q.; Wang, H.; Xu, G.-L.; Zhang, X.; Huang, D.; Fu, F.; Tang, Y.; Amine, K.; Shao, M. Structure-dependent performance of TiO_2/C as anode material for Na-ion batteries. *Nano Energy* **2018**, *44*, 217–227. [CrossRef]

32.	He, H.; Wang, H.; Sun, D.; Shao, M.; Huang, X.; Tang, Y. N-doped rutile TiO2/C with significantly enhanced Na storage capacity for Na-ion batteries. *Electrochim. Acta* **2017**, *236*, 43–52. [CrossRef]

33.	Gan, Q.; He, H.; Zhu, Y.; Wang, Z.; Qin, N.; Gu, S.; Li, Z.; Luo, W.; Lu, Z. Defect-assisted selective surface phosphorus doping to enhance rate capability of titanium dioxide for sodium ion batteries. *ACS Nano* **2019**, *13*, 9247–9258. [CrossRef] [PubMed]

34.	Fang, Y.; Zhang, Y.; Miao, C.; Zhu, K.; Chen, Y.; Du, F.; Yin, J.; Ye, K.; Cheng, K.; Yan, J. MXene-derived defect-rich TiO_2@ rGO as high-rate anodes for full Na ion batteries and capacitors. *Nano-Micro Lett.* **2020**, *12*, 128. [CrossRef]

35.	Opra, D.P.; Gnedenkov, S.V.; Sokolov, A.A.; Zheleznov, V.V.; Voit, E.I.; Sushkov, Y.V.; Sinebryukhov, S.L. Enhancing the reversible capacity of nanostructured TiO_2 (anatase) by Zr-doping using a sol–gel template method. *Scr. Mater.* **2015**, *107*, 136–139. [CrossRef]

36.	Blomgren, G.E. The development and future of lithium ion batteries. *J. Electrochem. Soc.* **2016**, *164*, A5019. [CrossRef]

37.	Zhang, Y.; Tang, Y.; Li, W.; Chen, X. Nanostructured TiO_2-Based Anode Materials for High-Performance Rechargeable Lithium-Ion Batteries. *ChemNanoMat* **2016**, *2*, 764–775. [CrossRef]

38.	Wang, M.; Zhang, F.; Lee, C.S.; Tang, Y. Low-cost metallic anode materials for high performance rechargeable batteries. *Adv. Energy Mater.* **2017**, *7*, 1700536. [CrossRef]

39.	Yu, S.-H.; Pucci, A.; Herntrich, T.; Willinger, M.-G.; Baek, S.-H.; Sung, Y.-E.; Pinna, N. Surfactant-free nonaqueous synthesis of lithium titanium oxide (LTO) nanostructures for lithium ion battery applications. *J. Mater. Chem.* **2011**, *21*, 806–810. [CrossRef]

40.	Ryu, M.-H.; Jung, K.-N.; Shin, K.-H.; Han, K.-S.; Yoon, S. High performance N-doped mesoporous carbon decorated TiO_2 nanofibers as anode materials for lithium-ion batteries. *J. Phys. Chem. C* **2013**, *117*, 8092–8098. [CrossRef]

41.	Pérez-Carvajal, J.; Aranda, P.; Obregón, S.; Colón, G.; Ruiz-Hitzky, E. TiO_2-clay based nanoarchitectures for enhanced photocatalytic hydrogen production. *Microporous Mesoporous Mater.* **2016**, *222*, 120–127. [CrossRef]

42.	Wang, Q.; Zhang, S.; He, H.; Xie, C.; Tang, Y.; He, C.; Shao, M.; Wang, H. Oxygen vacancy engineering in titanium dioxide for sodium storage. *Chem.–Asian J.* **2021**, *16*, 3–19. [CrossRef] [PubMed]

43.	Oliveira, N.; Guastaldi, A.C. Electrochemical stability and corrosion resistance of Ti–Mo alloys for biomedical applications. *Acta Biomater.* **2009**, *5*, 399–405. [CrossRef] [PubMed]

44.	Fujishima, A.; Zhang, X.; Tryk, D.A. TiO_2 photocatalysis and related surface phenomena. *Surf. Sci. Rep.* **2008**, *63*, 515–582. [CrossRef]

45.	Velten, D.; Biehl, V.; Aubertin, F.; Valeske, B.; Possart, W.; Breme, J. Preparation of TiO_2 layers on cp-Ti and Ti6Al4V by thermal and anodic oxidation and by sol-gel coating techniques and their characterization. *J. Biomed. Mater. Res. Off. J. Soc. Biomater. Jpn. Soc. Biomater.* **2002**, *59*, 18–28. [CrossRef]

46.	Motola, M.; Capek, J.; Zazpe, R.; Bacova, J.; Hromadko, L.; Bruckova, L.; Ng, S.; Handl, J.; Spotz, Z.; Knotek, P. Thin TiO_2 coatings by ALD enhance the cell growth on TiO2 nanotubular and flat substrates. *ACS Appl. Bio Mater.* **2020**, *3*, 6447–6456. [CrossRef]

47.	Ajmal, N.; Saraswat, K.; Bakht, M.A.; Riadi, Y.; Ahsan, M.J.; Noushad, M. Cost-effective and eco-friendly synthesis of titanium dioxide (TiO_2) nanoparticles using fruit's peel agro-waste extracts: Characterization, in vitro antibacterial, antioxidant activities. *Green Chem. Lett. Rev.* **2019**, *12*, 244–254. [CrossRef]

48.	Lewis, C.S.; Li, Y.R.; Wang, L.; Li, J.; Stach, E.A.; Takeuchi, K.J.; Marschilok, A.C.; Takeuchi, E.S.; Wong, S.S. Correlating titania nanostructured morphologies with performance as anode materials for lithium-ion batteries. *ACS Sustain. Chem. Eng.* **2016**, *4*, 6299–6312. [CrossRef]

49.	Wu, L.; Bresser, D.; Buchholz, D.; Passerini, S. Nanocrystalline TiO_2 (B) as anode material for sodium-ion batteries. *J. Electrochem. Soc.* **2014**, *162*, A3052. [CrossRef]

50.	Su, D.; Dou, S.; Wang, G. Anatase TiO_2: Better anode material than amorphous and rutile phases of TiO_2 for Na-ion batteries. *Chem. Mater.* **2015**, *27*, 6022–6029. [CrossRef]

51.	Gu, X.; Li, L.; Wang, Y.; Dai, P.; Wang, H.; Zhao, X. Hierarchical tubular structures constructed from rutile TiO_2 nanorods with superior sodium storage properties. *Electrochim. Acta* **2016**, *211*, 77–82. [CrossRef]

52. Hasegawa, G.; Kanamori, K.; Kiyomura, T.; Kurata, H.; Nakanishi, K.; Abe, T. Hierarchically porous Li₄Ti₅O₁₂ anode materials for Li-and Na-ion batteries: Effects of nanoarchitectural design and temperature dependence of the rate capability. *Adv. Energy Mater.* **2015**, *5*, 1400730. [CrossRef]

53. Li, Y.-N.; Su, J.; Lv, X.-Y.; Long, Y.-F.; Wen, Y.-X. Yeast bio-template synthesis of porous anatase TiO2 and potential application as an anode for sodium-ion batteries. *Electrochim. Acta* **2015**, *182*, 596–603. [CrossRef]

54. Hung, T.-F.; Lan, W.-H.; Yeh, Y.-W.; Chang, W.-S.; Yang, C.-C.; Lin, J.-C. Hydrothermal synthesis of sodium titanium phosphate nanoparticles as efficient anode materials for aqueous sodium-ion batteries. *ACS Sustain. Chem. Eng.* **2016**, *4*, 7074–7079. [CrossRef]

55. Li, Y.; Wang, S.; He, Y.-B.; Tang, L.; Kaneti, Y.V.; Lv, W.; Lin, Z.; Li, B.; Yang, Q.-H.; Kang, F. Li-ion and Na-ion transportation and storage properties in various sized TiO₂ spheres with hierarchical pores and high tap density. *J. Mater. Chem. A* **2017**, *5*, 4359–4367. [CrossRef]

56. Zhang, X.; Wang, M.; Zhu, G.; Li, D.; Yan, D.; Lu, T.; Pan, L. Porous cake-like TiO₂ derived from metal-organic frameworks as superior anode material for sodium ion batteries. *Ceram. Int.* **2017**, *43*, 2398–2402. [CrossRef]

57. Liu, X.; Xu, G.; Xiao, H.; Wei, X.; Yang, L. Free-standing hierarchical porous assemblies of commercial TiO₂ nanocrystals and multi-walled carbon nanotubes as high-performance anode materials for sodium ion batteries. *Electrochim. Acta* **2017**, *236*, 33–42. [CrossRef]

58. Li, H.; Zhang, Z.; Huang, X.; Lan, T.; Wei, M.; Ma, T. Metal–organic framework derived hierarchical porous TiO₂ nanopills as a super stable anode for Na-ion batteries. *J. Energy Chem.* **2017**, *26*, 667–672. [CrossRef]

59. Chu, C.; Yang, J.; Zhang, Q.; Wang, N.; Niu, F.; Xu, X.; Yang, J.; Fan, W.; Qian, Y. Biphase-interface enhanced sodium storage and accelerated charge transfer: Flower-like anatase/bronze TiO₂/C as an advanced anode material for Na-ion batteries. *ACS Appl. Mater. Interfaces* **2017**, *9*, 43648–43656. [CrossRef]

60. Wei, Z.; Wang, D.; Li, M.; Gao, Y.; Wang, C.; Chen, G.; Du, F. Fabrication of hierarchical potassium titanium phosphate spheroids: A host material for sodium-ion and potassium-ion storage. *Adv. Energy Mater.* **2018**, *8*, 1801102. [CrossRef]

61. Li, B.; Xi, B.; Feng, Z.; Lin, Y.; Liu, J.; Feng, J.; Qian, Y.; Xiong, S. Hierarchical porous nanosheets constructed by graphene-coated, interconnected TiO₂ nanoparticles for ultrafast sodium storage. *Adv. Mater.* **2018**, *30*, 1705788. [CrossRef] [PubMed]

62. Devina, W.; Nam, D.; Hwang, J.; Chandra, C.; Chang, W.; Kim, J. Carbon-coated, hierarchically mesoporous TiO₂ microparticles as an anode material for lithium and sodium ion batteries. *Electrochim. Acta* **2019**, *321*, 134639. [CrossRef]

63. Liu, Z.; Zhang, W.; Zhou, Z.; Liu, X.; Zhang, H.; Wei, M. Hierarchical porous anatase TiO₂ microspheres with high-rate and long-term cycling stability for sodium storage in ether-based electrolyte. *ACS Appl. Energy Mater.* **2020**, *3*, 3619–3627. [CrossRef]

64. Ma, J.; Xing, M.; Yin, L.; San Hui, K.; Hui, K.N. Porous hierarchical TiO₂/MoS₂/RGO nanoflowers as anode material for sodium ion batteries with high capacity and stability. *Appl. Surf. Sci.* **2021**, *536*, 147735. [CrossRef]

65. Xiong, Y.; Qian, J.; Cao, Y.; Ai, X.; Yang, H. Graphene-supported TiO₂ nanospheres as a high-capacity and long-cycle life anode for sodium ion batteries. *J. Mater. Chem. A* **2016**, *4*, 11351–11356. [CrossRef]

66. Ling, L.; Bai, Y.; Li, Y.; Ni, Q.; Wang, Z.; Wu, F.; Wu, C. Quick activation of nanoporous anatase TiO₂ as high-rate and durable anode materials for sodium-ion batteries. *ACS Appl. Mater. Interfaces* **2017**, *9*, 39432–39440. [CrossRef]

67. Yan, D.; Yu, C.; Bai, Y.; Zhang, W.; Chen, T.; Hu, B.; Sun, Z.; Pan, L. Sn-doped TiO₂ nanotubes as superior anode materials for sodium ion batteries. *Chem. Commun.* **2015**, *51*, 8261–8264. [CrossRef]

68. Opra, D.P.; Gnedenkov, S.V.; Sinebryukhov, S.L.; Gerasimenko, A.V.; Ziatdinov, A.M.; Sokolov, A.A.; Podgorbunsky, A.B.; Ustinov, A.Y.; Kuryavyi, V.G.; Mayorov, V.Y. Enhancing lithium and sodium storage properties of TiO₂ (B) nanobelts by doping with nickel and zinc. *Nanomaterials* **2021**, *11*, 1703. [CrossRef]

69. Xu, Y.; Lotfabad, E.M.; Wang, H.; Farbod, B.; Xu, Z.; Kohandehghan, A.; Mitlin, D. Nanocrystalline anatase TiO₂: A new anode material for rechargeable sodium ion batteries. *Chem. Commun.* **2013**, *49*, 8973–8975. [CrossRef]

70. Zhang, H.; Qin, B.; Buchholz, D.; Passerini, S. High-efficiency sodium-ion battery based on NASICON electrodes with high power and long lifespan. *ACS Appl. Energy Mater.* **2018**, *1*, 6425–6432. [CrossRef]

71. Jiang, N.; Hu, Y.; Jiang, H.; Li, C. Hierarchical TiO₂ microspheres with enlarged lattice spacing for rapid and ultrastable sodium storage. *Chem. Eng. Sci.* **2021**, *231*, 116298. [CrossRef]